EBioMedicine 70 (2021) 103529

Contents lists available at ScienceDirect

EBioMedicine

journal homepage: www.elsevier.com/locate/ebiom

In situ DESI-MSI lipidomic profiles of mucosal margin of oral squamous cell carcinoma

Xihu Yang, Dr.[a,b,1,*], Xiaowei Song[c,1], Xiaoxin Zhang[d], Vishnu Shankar[e], Shuai Wang[b], Yan Yang[f], Sheng Chen[f], Lei Zhang[f], Yanhong Ni, Dr.[d], Richard N. Zare, Dr.[c,e], Qingang Hu, Dr.[b]

[a] Department of Oral and Maxillofacial Surgery, Affiliated Hospital of Jiangsu University, Zhenjiang, Jiangsu, 210008, China
[b] Department of Oral and Maxillofacial Surgery, Nanjing Stomatological Hospital, Medical School of Nanjing University, Nanjing, Jiangsu, 210000, China
[c] Department of Chemistry, Fudan University, Shanghai, 200438, China
[d] Central Laboratory of Stomatology, Nanjing Stomatological Hospital, Medical School of Nanjing University, Nanjing, Jiangsu, 210000, China
[e] Department of Chemistry, Stanford University, Stanford, California, 94305, USA
[f] Department of Oral Pathology, Stomatological hospital, Medical School of Nanjing University, Nanjing, Jiangsu, 210000, China

ARTICLE INFO

Article History:
Received 9 January 2021
Revised 15 July 2021
Accepted 28 July 2021
Available online xxx

Keywords:
OSCC
DESI-MSI
Lipidomics
Surgical margin
Surgical resection distance

ABSTRACT

Background: Although there is consensus that the optimal safe margin is ≥ 5mm, obtaining clear margins (≥5 mm) intraoperatively seems to be the major challenge. We applied a molecular diagnostic method at the lipidomic level to determine the safe surgical resection margin of OSCC by desorption electrospray ionisation mass spectrometry imaging (DESI-MSI).

Methods: By overlaying mass spectrometry images with hematoxylin-eosin staining (H&E) from 18 recruited OSCC participants, the mass spectra of all pixels across the diagnosed tumour and continuous mucosal margin regions were extracted to serve as the training and validation datasets. A Lasso regression model was used to evaluate the test performance.

Findings: By leave-one-out validation, the Lasso model achieved 88.6% accuracy in distinguishing between tumour and normal regions. To determine the safe surgical resection distance and margin status of OSCC, a set of 14 lipid ions that gradually decreased from tumour to normal tissue was assigned higher weight coefficients in the Lasso model. The safe surgical resection distance of OSCC was measured using the developed 14 lipid ion molecular diagnostic model for clinical reference. The overall accuracy of predicting tumours, positive margins, and negative margins was 92.6%.

Interpretation: The spatial segmentation results based on our diagnostic model not only clearly delineated the tumour and normal tissue, but also distinguished the different status of surgical margins. Meanwhile, the safe surgical resection margin of OSCC on frozen sections can also be accurately measured using the developed diagnostic model.

Funding: This study was supported by Nanjing Municipal Key Medical Laboratory Constructional Project Funding (since 2016) and the Centre of Nanjing Clinical Medicine Tumour (since 2014).

1. Introduction

Oral squamous cell carcinoma (OSCC) is one of the most common head and neck cancers and causes nearly 177.400 deaths worldwide annually [1]. Although OSCC treatments have improved over the past few decades, the survival rate has not increased significantly because of the high recurrence rate [2]. Difficulty in obtaining 'clear' resection margins, which results in local recurrence, is the main reason for OSCC surgical treatment failure. Margins containing tumour cells or dysplastic epithelium, i.e., positive margins, will lead to higher local recurrence rates of OSCC [3-6]. Our team reported that patients with remaining mild dysplasia margins after excision had a worse prognosis than those with negative margins [7]. Therefore, it is urgent to know the safe surgical margin distance intra-operatively to guide surgical decisions. Currently, the adequacy of the surgical margin can only be determined by the postoperative HE paraffin section, which does not allow guidance during the operation.

* Department of Oral and Maxillofacial Surgery, Nanjing Stomatological Hospital, Medical School of Nanjing University, Nanjing, Jiangsu 210000, China; Department of Chemistry, Stanford University, Stanford, California 94305 USA; Central Laboratory of Stomatology, Nanjing Stomatological Hospital, Medical School of Nanjing University, Nanjing, Jiangsu 210000, China
E-mail addresses: yangxihu1981@126.com (X. Yang), Niyanhong12@163.com (Y. Ni), rnz@stanford.edu (R.N. Zare), qghu@nju.edu.cn (Q. Hu).
[1] Xihu Yang and Xiaowei Song contributed equally to this work.

https://doi.org/10.1016/j.ebiom.2021.103529

Research in context

Evidence before this study

Obtaining negative surgical margins and safe excisional margin distance during surgery has always been the pursuit of oncologic surgeons. According to the NCCN guidelines, the safe margin distance for oral squamous cell carcinoma (OSCC) is recommended to be ≥5 mm, but the 5-mm cut-off is obtained from the postoperative paraffin section, which limits real-time guidance. Moreover, a rate of positive surgical margin as high as 12.75% after surgery has been reported by HE paraffin section, suggesting that the method of intraoperative margin determination needs to be improved. In the past few years, DESI-MSI has showed its emerging potential in clinical applications such as the accurate assessment of surgical margin status in gastric and pancreatic cancer during surgery. Therefore, we aimed to identify the safe surgical resection distance and margin status of OSCC using desorption electrospray ionisation mass spectrometry imaging (DESI-MSI).

Added value of this study

We consider our finding to represent some advance in the ability to determine the safe margin distance of OSCC by oncolipid signalling. In our study, we were able to detect minimal residual cancer cells and determine the molecular safe margin distance of OSCC, all of which were achieved by combining DESI-MSI with machine learning. We were able to accurately measure the safe surgical resection margin of OSCC within 30 min per sample during surgery and make a diagnosis for different margin status.

Implications of all the available evidence

It is important that the surgeon be informed of the adequacy of the surgical margin intra-operatively. Currently this is determined by the postoperative HE paraffin section, which does not allow guidance during the operation. Evaluation of the safe margin distance of OSCC at the molecular level during surgery is a promising new molecular diagnostic method that can effectively supplement the traditional pathological evaluation.

The gold standard for assessing OSCC surgical margins is histopathological evaluation by a pathologist using a microscope, but patients with histologically negative margins still have the possibility of recurrence [7]. In addition, a rate of positive surgical margins as high as 12.75% after surgery has been reported by HE paraffin section [8], suggesting that the method of intraoperative margin determination needs to be improved. For example, the number and location of surgical margins obtained by surgeons intra-operatively are random and subjective. Moreover, the histopathological assessment of the frozen section only reflects the morphological changes of the cells and does not reflect the underlying molecular alterations. Therefore, the concept of molecular margins has been introduced to supplement traditional pathological methods [9-14]. However, determining the safe margin distance during the operation is especially urgent for surgeons. Recently, with the advancement of basic and clinical research on the surgical margin of OSCC, the focus has shifted from margin status to margin distance. According to the National Comprehensive Cancer Network (NCCN) guidelines, the safe margin distance for OSCC is recommended to be ≥5 mm, but the 5-mm cut-off is obtained from the postoperative paraffin section, which prevents real-time reconstruction. Our previous study also found that molecular markers were different at different distance of surgical margin of OSCC, which confirmed that metabolic molecular differences exist at different surgical margins [15]. However, it is urgent to determine the safe margin of OSCC using in situ imaging, which can guide accurate resection intra-operatively.

In the last few years, ambient ionisation mass spectrometry (AIMS) has become a powerful tool for multiplex tissue imaging and chemical diagnosis [16-19]. Unlike the conventionally used liquid/gas chromatography-mass spectrometry systems (LC/GC-MS), AIMS enables direct, multiplex chemical analysis at the tissue level without any labour-intensive sample pre-treatment steps. Therefore, endogenous lipid molecule information can be intactly preserved with no spatial information loss. Among the reported AIMS techniques, desorption electrospray ionisation mass spectrometry imaging (DESI-MSI) has become one of the most widely used ones because of its robustness, affordability, low cost, and convenient operation under atmospheric conditions. Principally, the metabolic and lipidomic profile information in a very tiny tissue region (approximately 50 μm × 50 μm) can be easily transferred into the mass spectrometer by the charged solvent microdroplets introduced by a coaxial capillary system aided by the nebulising gas and high voltage [20].

DESI-MSI can not only collect a wide array of detectable chemical species (amino acids, nucleotides, lipids, carbohydrates, peptides, and drugs) simultaneously, but can also separately provide each component's spatial information on microregion distribution. Therefore, a single DESI-MSI experiment on a tissue is equivalent to hundreds of histological chemistry tests. In the past few years, its emerging potential in clinical applications such as the accurate assessment of surgical margin status in gastric and pancreatic cancer during surgery has already been proven [21,22]. These studies mainly focused on the identification of margin status, whereas OSCC requires more accurate identification of the margin distance because of its special anatomic location (that is, the space and the surgical resection distance is limited). The authors are unaware of a previous study that determined the safe margin distance of OSCC during surgery with the aid of DESI-MSI combined with Lasso regression. Our research provides metabolic molecular support for the determination of safe margin distance of OSCC.

2. Methods

2.1. Participants and tumour specimens

This study was approved by the Medical Ethics Committee of Nanjing Stomatology Hospital, Medical School of Nanjing University. A total of 22 participants were recruited, and all participants signed informed consent forms (NJSH-2021NL-50). The inclusion criterion was that the participants with primary OSCC had received radical surgery at the Nanjing Stomatology Hospital and Affiliated Hospital of Jiangsu University. We only collected the superficial mucosal margin for DESI-MSI analysis. Eighteen of the 22 participants had continuous mucosal margins of sufficient length. In the other four participants, the margins were discontinuous, but the tumour and normal regions remained. All tissues were frozen in liquid nitrogen and stored in a −80°C freezer until cryosectioned (10 μm thick) using a Leica CM1950 cryostat (Leica Microsystems). The cryosectioned tissue was then thaw-mounted on glass slides and stored in a −80°C freezer until use. The tissue sections were then dehydrated in a desiccator under vacuum for approximately 15 min before DESI-MSI.

2.2. Histopathological examination of tissues

Two parallel cryosectioned tissues (labels #1 and #2) were analysed by histological evaluation or subjected to DESI-MSI analysis. After a standard H&E staining protocol, the tissue composition and continuity of the margins were evaluated under a microscope (Olympus, Tokyo, Japan) by two expert pathologists (Prof. XF. Huang and L.

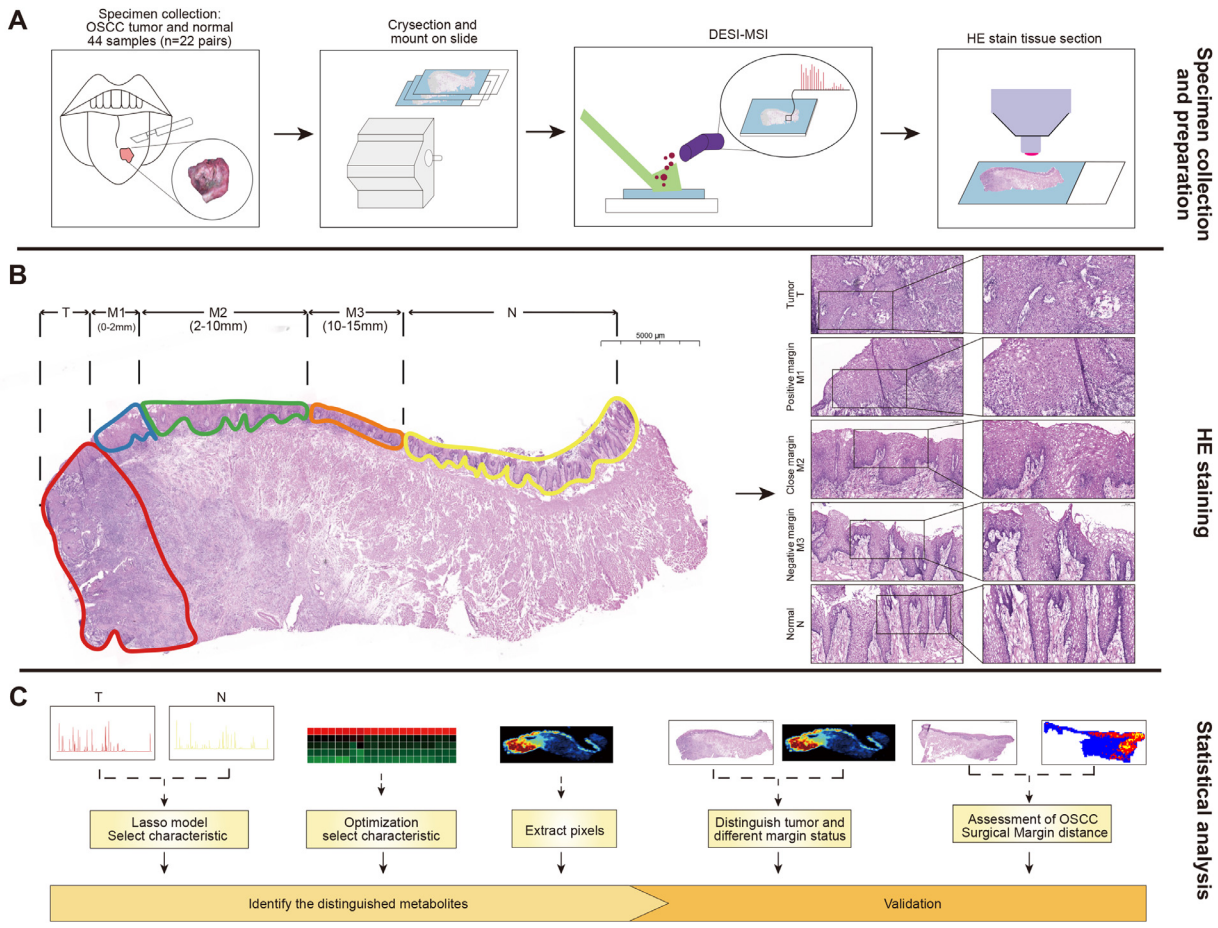

Fig. 1. The schematic illustration of the general workflow of this research. a. Sample collection (n=22), frozen section preparation (n=22), DESI-MSI analysis (n=3). **b.** H&E staining of the whole tissue (contain tumor and margin) which were divided into five parts: Tumor (T), M1 (positive margin, 0-2 mm), M2 (close margin, 2-10 mm), M3 (negative margin, 10-15 mm), Normal tissues (>15 mm). **c.** Machine learning model development, statistical analysis, and biological validation.

Zhang According to previous reports and our study **(Fig. S4)**, the shrinkage rate between fresh frozen tissue and paraffin tissue is approximately 50% to 60% (**Table S6**)(23, 24). Therefore, we redefined different margin status (mucosa margin) in the frozen section: positive margin (M1 region, 0–2 mm), close margin (M2 region, 2–10 mm), and negative margin (M3 region, > 10 mm), and N (normal tissue > 15 mm) (**Fig. 3A**). Eighteen of the 22 participants' tissues which had tumours and continuous margins (sufficient lengths > 15 mm) were divided into five parts annotated as follows: T (tumour regions), M1 (0–2 mm), M2 (2–10 mm,), M3 (>10 mm, negative margin), and N (normal tissue > 15 mm) (**Fig. 1**). M1, M2, M3, and N were classified according to the pathological classification of surgical margins and tissue shrinkage. Specimens with continuous surgical margins were used to measure the margin distance and evaluate margin status. For the remaining four specimens with discontinuous margins (**Fig. S1**), only the T and N regions were selected, together with the pairs of T and N regions from the other 18 specimens for molecular model development.

2.3. DESI-MSI analysis

A 2D DESI source (Prosolia, Indianapolis, IN, USA) coupled to an LTQ Orbitrap Elite mass spectrometer (Thermo Fisher Scientific, San Jose, CA, USA) was used for tissue molecular imaging (**Fig. S2**). The tissue section was scanned by the DESI sprayer which consisted of two coaxial capillaries for spraying solvent and nebulising gas transport. The outer capillary is made of stainless steel (ID: 150 μm). The inner capillary is made of silicate (OD: 100 μm, ID: 50 μm). A mix of organic solvents was aspirated using a syringe pump into the inner capillary channel. Nitrogen gas (99.5%) was introduced into the outer capillary channel. A high voltage supplied endogenously from the mass spectrometer was applied to the DESI sprayer. With the aid of direct current high voltage and nitrogen gas, charged solvent droplets were formed when the solvent was removed from the sprayer outlet. These charged droplets impact the tissue and carry the extracted tissue components instantly into the transport tube-linked mass spectrometer for complete data recording. DESI-MSI was performed in negative ion mode within the range of *m/z* 200–1000. The MS capillary temperature was set at 275°C and the S lens voltage was 55 V. Dimethyl formamide acetonitrile (1:1, *v/v*) was formulated as the spray solvent system at a flow rate of 2.0 μL/min was applied under -4 kV high voltage and 1.0 MPa nebuliser gas pressure. Whole tissue cryosections were scanned line-by-line using a DESI sprayer. The lateral scan speed (in the X-axis direction) was set at 300 μm/sec. The inter-line interval (Y-direction) was set at 300 μm. The DESI geometry parameters were as follows: the impact angle and distance between the sprayer tip and substrate were 55° and 4.5 mm, respectively. The tip-to-collection tube distance was 4.5 mm. The height of the collection tube to the substrate was 0.5 mm. More details about the schematic DESI geometry and commercial device can be found in the supplementary information and previous reports [21].

2.4. Lipidomics data processing

The commercial format of raw data files obtained by DESI-MSI was first converted into the commonly accessible date format cdf files using Xcalibur (Thermo Fisher Scientific, San Jose, CA, US). Massimager (Chemmind Technologies, Beijing, China) was employed for the

construction of ion images and co-localisation with the optical image of H&E staining [25,26]. The ion images were plotted and manually segmented into regions of interest (five regions), as determined by histopathological evaluation. Under co-localisation of the MS image with the H&E staining image, each pixel's accurate assignment was precisely labelled for model development. Further procedures were conducted using the MATLAB 2019 platform (Mathworks, Natick, MA, USA) and Rstudio with self-written processing scripts. A sample matrix for the statistical test and machine model development was constructed with each row representing one pixel in a selected region and each column representing one ion in the mass spectrum. Total ion current normalisation and natural logarithm transformation were carried out to remove the inter-mass spectra response fluctuation and convert the data into a multivariate normal distribution. The entire pre-processed data matrix was then saved into a csv file for further statistical analysis using the glmnet package (**Fig. S3**).

2.5. Lasso regression modelling

To realise the automatic and unbiased prediction of the tissue types at the precision of the pixel basis, a machine learning model was further developed in this study. Specifically, we initially used all the peaks acquired by the untargeted DESI-MSI scanning to train the pixel-based Lasso regression model. The Lasso regression modelling process (binary logistic regression with L1 penalty) was implemented using the glmnet package in the CRAN R language library [27]. To distinguish normal and tumour regions based on the abundance of molecular species from the DESI-MSI profile, we first pre-processed the data, converting the raw files into csv files before reading the pixel-level data to the R language. To account for peak shifting between specimens, we used the nearest neighbour clustering method to collect all pixel intensities corresponding to the nearest mass spectra. The training set consisted of 22,955 metabolite peaks from 7,243 pixels, which were labelled as T (tumour) or N (normal). Based on the processed DESI-MSI data, we applied the Lasso method [28] to find the most informative lipid ions that could accurately predict the class of a pixel (either normal or tumour) from the relative abundances of selected molecular species. Leave-one-patient-out cross-validation was used to assess the accuracy of the model performance.

2.6. Immunohistochemistry

Immunohistochemistry (IHC) was used to detect monoclonal mouse anti-p53 (Abcam, UK) in margin sections from all 18 participants according to the manufacturer's protocol, and PBS and normal margins were used as negative controls. Tissues were formalin-fixed, paraffin-embedded, cut into 3 μm sections and placed on microscope slides for IHC. In brief, the sections were successively incubated in xylene, 100% ethanol, 95% ethanol, blocked with 3% H_2O_2 for 10 min at room temperature, and washed. Then, all slides were incubated with a P53 primary antibody at 4°C overnight, followed by secondary antibody, and the Envision Detection System kit was used for the DAB chromogen, followed by nuclear staining using haematoxylin. For the specific IHC steps, please refer to our previous report.

2.7. Statistical Analysis

After a Lasso model was developed for automatic margin prediction, the highly contributing lipid ion was selected as the characteristic marker according to its absolute value of the weight coefficient in the model. The average intensities of each characteristic marker in the tumour (T) and normal (N) regions were compared using a non-parametric hypothetical test due to their uncertain data distributions. The statistical significance of characteristic markers was evaluated using the Mann–Whitney U test (rank sum test). Initially, there were 36 pairs in total of T and N regions from intact OSCC tissues harvested from the bedside surgery. Through cryo-sectioning and pathological examination, 18 tissues with intact margins consisting of of T, M1, M2, M3, and N regions were included for statistical testing. No randomness or blinding strategy was employed until the marker stage and model validation. Receiver operating characteristic curve analysis was conducted to evaluate the diagnostic performance of characteristic lipids, with the area under the curve as the metric. All statistical analyses were conducted using GraphPad Prism 8 (GraphPad Software, San Diego, CA, USA).

2.8. Data Availability

The datasets generated and/or analysed during the current study are available from the corresponding author upon reasonable request.

2.9. Role of funding source

The funders were not involved in study design, data collecting, analysis, interpretation, decision to publish or writing of the manuscript. The corresponding author Qingang Hu had full access to all the data in the study and had final responsibility for the decision to submit the manuscript for publication.

3. Results

3.1. Clinical Characterisation of OSCC tissues and DESI-MSI analysis

The entire flowchart of the study is illustrated schematically in **Fig 1**. A total of 22 human OSCC tissue specimens containing tumour tissue and surgical margin tissue prospectively collected from surgeries for this study were scanned by DESI-MSI in the negative ion mode. The clinical information of the 22 participants is shown in **Table S1.** Eighteen of the 22 participants had continuous and sufficient length margins **(Fig. 1b),** and the margins of another four participants were discontinuous but contained tumour and normal tissue **(Fig. S1).** Each continuous specimen was divided into five parts (T, M1, M2, M3, and N) according to the pathological classification of the surgical margin and tissue shrinkage for DESI-MSI analysis **(Fig. 1b).** In the machine learning model development stage and indicative marker discovery, only pixels in the T and N regions were selected. Other regions, such as muscle tissues, were not included in our study. For most of the specimens, evaluation of the 2D DESI-MSI images revealed molecular heterogeneity within the different regions. As shown in **Fig. 2a**, regions of T and M1 displayed higher relative abundances of lipids in the higher mass range (m/z 600–900) than M2, M3, and N, indicating that there was significant lipidomic variation among different margin distances.

3.2. Screening discriminating lipid ions for margin evaluation by Lasso model

A total of 22,955 peaks were discovered as feature candidates collected across 7,243 pixels (**Fig. S3**). Finally, the optimal Lasso model selected 179 of these 22,955 peaks as features (**Table S2**). To go from the pixel-level to tissue-level classification, a simple majority rule was used, where if over 50% of pixels in a tissue were predicted to be cancerous, the entire tissue was predicted to be cancerous. **Table S3** summarises the cross-validation performance of Lasso. Notably, the model achieved an overall accuracy of 88.6% with 81.8% sensitivity (true positive rate) and 95.5% specificity (true negative rate). Although Lasso has been successfully used in previous efforts to distinguish between healthy and cancerous pixels [29], we also tested a decision tree model, which is known to capture non-linear decision boundaries between groups. We found that this approach achieved

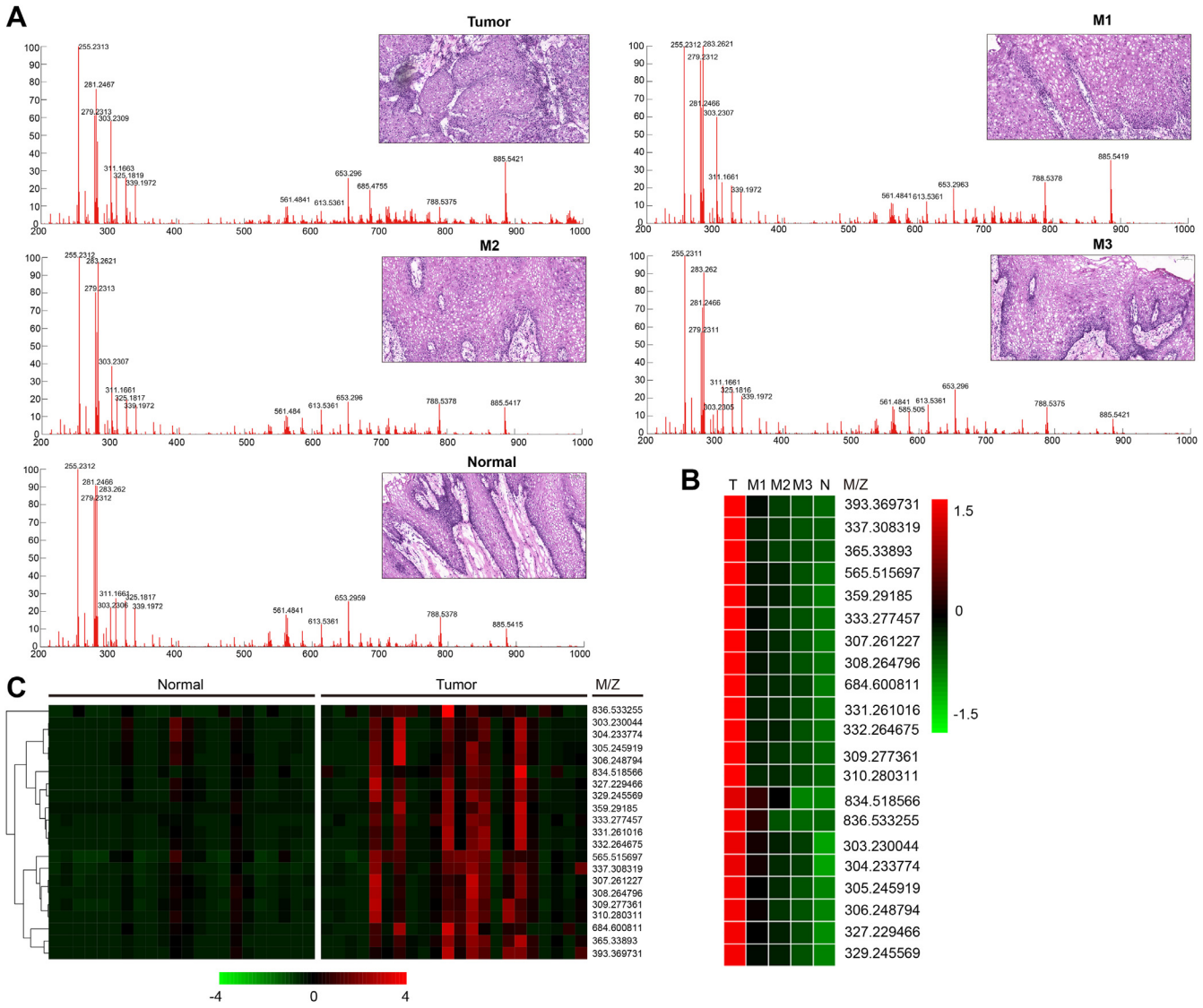

Fig. 2. Representative mass spectral profiles and significantly changed ions between tumor, continuous margin and the normal tissue. a. Tumor tissue, positive margin, close margin, negative margin, and normal tissues mass spectra analysis. **b.** Heat map analysis of 21 differential ions showed a gradual decrease from tumor to normal tissue (average ion strength in each group). **c.** The intensity of 21 different ions in each sample of tumor and normal tissues (heat map analysis) can distinguish tumors from normal tissues (n=22 pairs).

significantly lower cross-validation accuracy (**Table S4**). Moreover, the Lasso prediction can accurately identify the tumour, the inadequate margin, and the normal region located at different margin distances (Fig. 3), and the predicted results are highly consistent with those of pathological diagnosis by H&E staining.

Although a panel of 179 characteristic features was selected without bias by assigning them with higher weight coefficients in the Lasso model, our ultimate goal was to identify the most important ions that function as discriminating markers for margin distance and status assessment. Therefore, we further screened these ions which tended to gradually increase or decrease along with the increase in distance from tumour to normal. Among 179 characteristic features, there were 21 gradually increasing or decreasing lipid ions from the tumour to normal tissues. Heatmap visualisation showed that the 21 metabolites decreased gradually from tumour to normal tissues of the 18 participants who had margins that were continuous and of sufficient length (Fig. 2**b**). Moreover, these 21 discriminating metabolite ions effectively distinguished 22 paired tumours from normal tissues (Fig. 2**c**). After further confirmation with the reconstructed ion image, seven isotope peaks and false positive peaks (background ions) were excluded. Finally, 14 decreasing ions were ultimately selected as indicative markers for determining the margin distance. (**Table S5**).

3.3. Assessment of tumour and surgical margin status using established diagnostic model

Clinically, the rapid diagnosis of OSCC surgical margin status is mainly based on the pathological diagnosis of intraoperative frozen sections. The practitioner not only needs to quickly discern the tumour and normal regions but also precisely delineate the positive and negative margins. Therefore, we continued to test the feasibility of precise molecular assessment of the margin status using the 14 lipid ions described above. Eighteen frozen sections which preserved continuous margin regions (M1, M2, and M3) were further investigated. As shown in Fig. 3**a-p**, there were clear differences in the distribution and abundance of the 14 ions. The overlay image of the 14 ion images clearly distinguished the tumour from the margin tissues.

According to previous reports and our study (**Fig. S4**), the shrinkage rate between fresh frozen tissue and paraffin tissue is

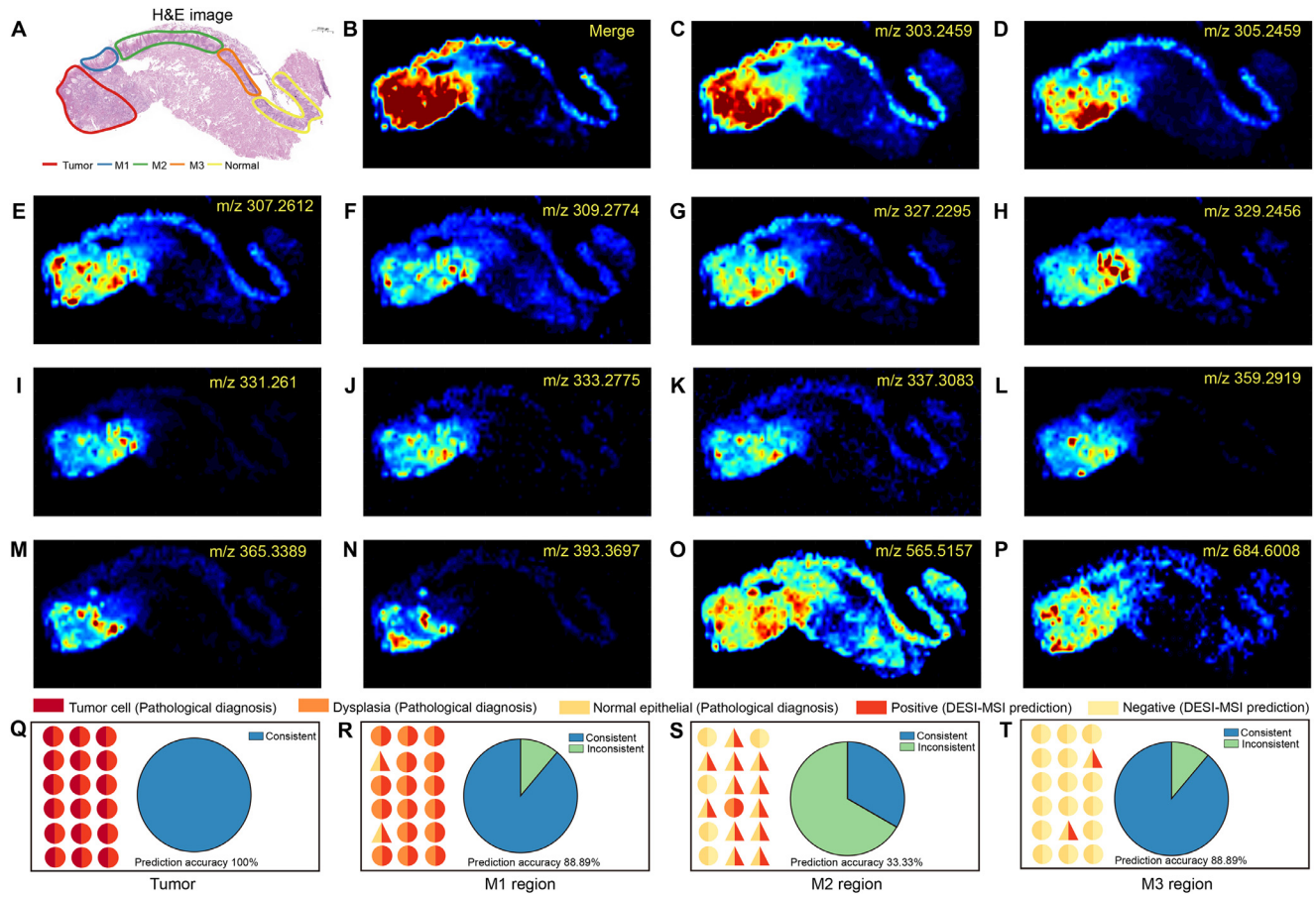

Fig. 3. Different surgical margin status determined by 14 characteristic lipid ions' images and their merged image. A. H&E staining of frozen section, we redefined different margin status in the frozen section: positive margin (M1 region, 0-2 mm), close margin (M2 region, 2-10 mm), and negative margin (M3 region, > 10 mm) according the shrinkage rate between fresh frozen tissue and paraffin tissue. **b**. The merge of the 14 characteristic lipid ion images in the case**. c-p.** Separate image of the characteristic lipid ions. **q-t.** Prediction results given by the DESI-MSI for tumor, M1, M2, M3 region (n=18 cases) compared with pathological diagnosis. Circle: the DESI-MSI prediction is consistent with the pathological results; Triangle: the DESI-MSI prediction is not consistent with the pathological results. Pathological diagnosis include tumor, dysplasia, normal epithelial; DESI-MSI prediction include positive (red bright spot) and negative (non-red bright spot).

approximately 50% to 60% (**Table S6**)(23, 24). Therefore, we redefined margin status (mucosa margin) in the frozen section as: positive margin (M1 region, 0−2 mm), close margin (M2 region, 2−10 mm), and negative margin (M3 region, > 10 mm) (**Fig. 3a**). We used the diagnostic model to directly predict tumours and different margin statuses in the frozen sections, followed by cross-validation by pathological diagnosis results. The results showed that the prediction accuracy of the tumour, positive margin (M1 region), and negative margin (M3 region) reached 100%, 88.89%, and 88.89%, respectively (**Fig. 3q, r, t**). For close margins (M2 region), there was only 33.3% (6/18) accuracy (**Fig. 3s, Table S7**), and these results showed a wide range of fluctuation in OSCC safe margin distance; individual measurements are needed.

According to the worst pattern of invasion (WPOI) classification, a total of five cases were WPOI-5 (Table S1); that is, the small satellite foci were greater than 10 mm from the tumour nest. Interestingly, we also observed tiny lesions far from the cancer nests by DESI-MSI (Fig. S6) in 3 WPOI-5 cases (3/5). We need to recruit more samples for deep margin studies.

3.4. Individualised assessment of OSCC safe margin distance by established DESI-MSI diagnostic Model

Different sites and clinical stages of OSCC may have different safe margin distances. In this study, we used a DESI-MSI-based diagnostic model to determine the safe margin distance of OSCC and compared it with the traditional pathological assessment method. As shown in **Fig. 4 a-d,** according to the overlay image composed of 14 separate ion images, the safe surgical resection distance was determined in the frozen section **(Table S6).** The DESI-MSI safe surgical resection distance of most lesions was located in the close margin region (M2 region), and only two lesions were located in the negative margin region (M3 region) (**Fig. 4e**). Further analysis confirmed that most of the safe surgical resection margin boundaries delineated by DESI-MSI were pathologically negative (17/18, 94.4%, **Table S8).** Interestingly, our diagnostic model accurately delineated a positive surgical margin in one lesion (**Fig. 5**), where the positive margin extended from the tumour boundary to the negative margin (DESI-MSI margin distance: 7.9 mm). These results showed that the DESI-MSI-based lipid-molecular margin has a powerful application potential for the individualised evaluation of OSCC margins. It may detect suspicious areas on a lipid-molecular level that cannot be easily recognised by traditional histological methods.

To verify the accuracy of the safe margin range determined by DESI-MSI, we further corroborated it at the genetic molecular level. According to previous studies [30,31], p53 has been determined to be a molecular marker of the margin of OSCC; therefore, we detected the expression of p53 in the surgical margin and compared it with the safe surgical resection range determined by DESI-MSI. As shown in **Fig. 6**, the safe margin boundary determined by DESI-MSI and p53 was highly consistent.

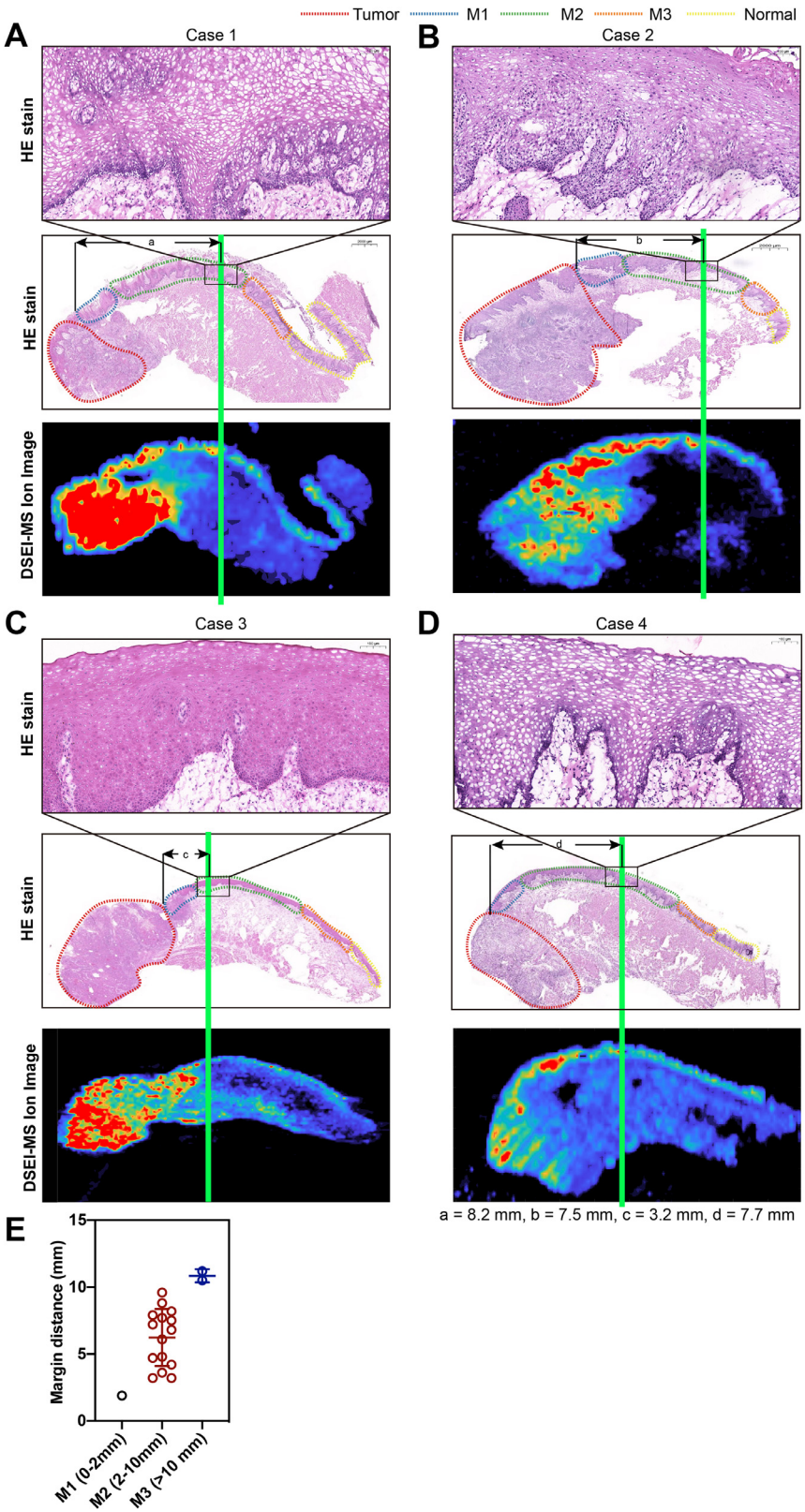

Fig. 4. Safe margin distance of OSCC determined by DESI-MSI/Lasso model (Called "DESI-MSI Margin"). a-d. the mass spectrometry images clearly depicts the safe margin distances in 4 cases. For each case: **Up:** H&E staining of safe margin boundary (10 X). **Middle:** H&E staining of frozen sections. **Down:** Mass spectrometry images of the same frozen section. The region where the image intensity decreases or disappears is defined as the safe margin boundary. **e:** Distribution of the margin distances in M1, M2, and M3 regions among the collected eighteen OSCC tissues.

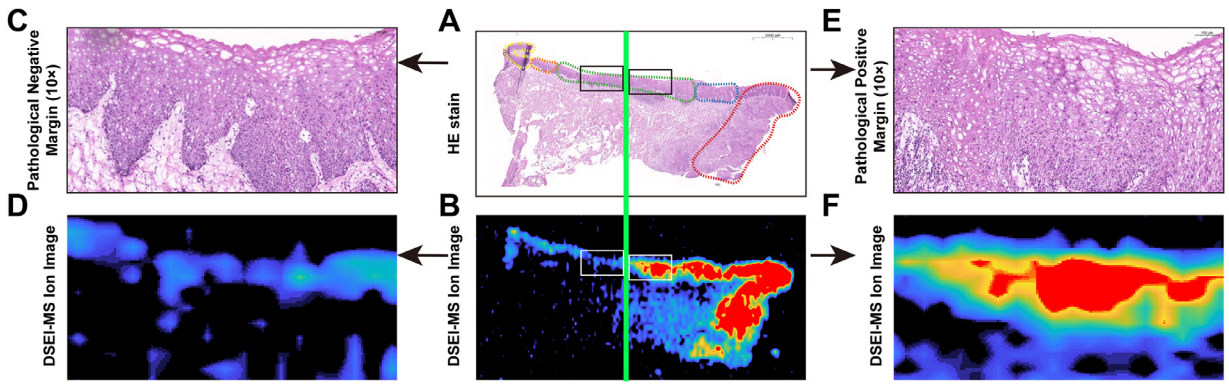

Fig. 5. The diagnostic model delineates the positive margin boundary. a. H&E staining of frozen section. **b**. The merge image of the 14 characteristic lipid ions for the same frozen section. **c.** The histopathological diagnosis of "DESI-MSI negative margin" was finally confirmed as negative surgical margin. **d.** The locally enlarged merge image of the 14 characteristic lipid ions for delineating the "DESI-MSI negative margin". **e.** The histopathological diagnosis of "DESI-MSI positive margin" was finally confirmed as dysplasia margin. **f:** The locally enlarged merge image of the 14 characteristic lipid ions for delineating the "DESI-MSI positive margin".

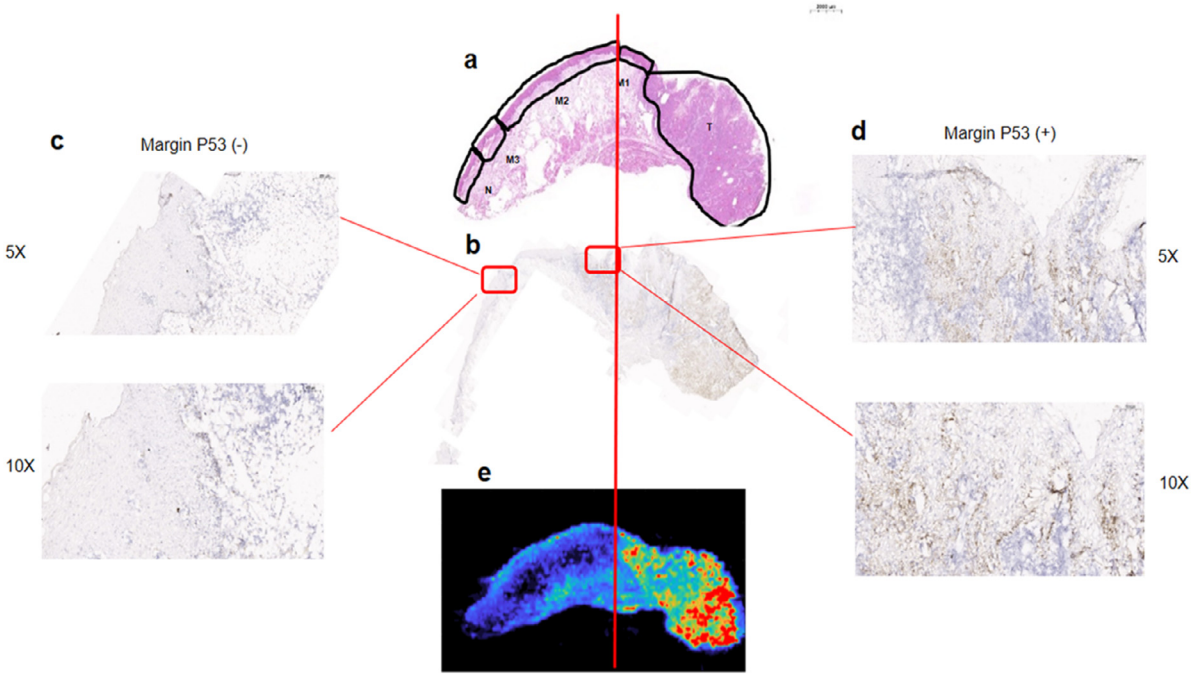

Fig. 6. Genetic marker P53 validate the safe surgical-resection range determined by DESI-MSI. a, H&E staining of frozen section. **b-d**, Immunohistochemical stain of p53 on the same frozen section. **e**, DESI-MSI analysis of the same frozen section.

4. Discussion

The main reason for OSCC treatment failure is local recurrence caused by the difficulty in obtaining 'clear' resection margins based merely on cell morphological patterns [32,33]. Thus, the concept of molecular margins was introduced to more accurately characterise the profile changes along the margin regions. In recent decades, genomic and proteomic studies have identified the molecular surgical margins of OSCC [30-33]. The carcinogenic potential of these upstream molecules has been well elucidated and has been shown to be associated with prognosis. We previously reported that p53 expression levels in dysplastic surgical margins are correlated with early OSCC recurrence [34]. However, most studies on molecular margins have been restricted to a single gene or protein marker, and this information cannot provide a precise diagnosis of specific margin status. Margins characterised by multiplex molecular combinations can more effectively predict margin status. Therefore, a panel of amino acids as a marker group for negative margins and dysplastic margins was reported in our previous work using GC-MS and ultra-high performance liquid chromatography-tandem mass spectrometry [15].

With the advancement of clinical research on the surgical margin of OSCC, the focus has gradually moved from margin status to margin distance. In 1998, the Royal College of Pathologists issued guidelines for dividing margins into involved ($<$ 1 mm), close (1–5 mm), or clear ($>$ 5 mm) in paraffin sections, and this classification has been widely adopted [35]. However, the 5-mm cut-off for demarcation between the involved and close is controversial. The use of other OSCC margin cut-offs, such as 3 mm or 2.2 mm, has been investigated, showing significant prognostic ability [11-14]. Thus, the safe margin distance of OSCC needs to be further studied and validated at the molecular level.

The purpose of the present study was to evaluate the margin distance of OSCC in fresh frozen sections. DESI-MSI is one of the most widely used ambient ionisation MS techniques and has been used to analyse fresh specimens directly on frozen sections. Our team and

other researchers have used the DESI-MSI technique to accurately evaluate the margin status of cancers during surgery, such as gastric cancer, prostate cancer, breast cancer, brain tumours, and pancreatic cancer [36-41]. Because of the specific anatomic subsites of OSCC, it is necessary to accurately determine the safe margin distance and status during the operation. In the present study, we used DESI-MSI to examine frozen sections collected from 22 OSCC specimens which contained tumour tissue and surgical margins. A diagnostic model consisting of 14 significantly changed ions was selected using the Lasso model to determine the margin status and margin distance. The selected lipid ions in the diagnostic model were first tentatively identified as fatty acids and fatty acid esters of hydroxy fatty acids (**Table S9**) through HR-MS searching in the human metabolome database (HMDB, http://www.hmdb.ca/spectra/ms/search) and lipid maps (https://www.lipidmaps.org/). Then, the CID-MS2 experiment was performed to further confirm the metabolite species (**Table S10**).

Accurate intraoperative evaluation of OSCC surgical margin status is critical for improving overall surgical success and patient survival. According to the shrinkage rate between fresh tissue and paraffin tissue [23,24], we redefined the different mucosal margin status on fresh frozen sections. The prediction accuracy of our model for tumour, mucosa positive margin, and mucosal negative margin reached 100 %, 88.9 %, and 88.9 %, respectively. The overall prediction accuracy of the tumour, positive margin, and negative margin was 92.6 %. The exact distance of the close margin in the pathology and surgery fields is controversial because of its large distance span. Our prediction model showed that 66.7 % (12/18) of the positive margins in DESI-MS images were in the close margin group. Moreover, we also observed tiny lesions far from the cancer nests in the deep margin by DESI-MSI. These results indicate that our diagnostic model may individually distinguish different margin statuses, involving both the mucosa and deep margins.

Accurate measurement of safe margin distance during OSCC surgery has important clinical implications. The gold standard is H&E staining of formalin-fixed paraffin-embedded tissue sections, which typically requires a few days to complete. Currently, techniques used for intraoperative margin assessment of OSCC mainly include Mohs micrographic surgery, molecular analysis, non-fluorescent dyes, fluorescent dyes, auto-fluorescent imaging, narrow-band imaging, narrow-field analysis (elastic scattering spectroscopy and Raman spectroscopy), optical coherence tomography, etc. However, these techniques lack in-depth information support at the molecular level. Such as, Raman spectroscopy distinguishes tumors from normal tissue based on the content of water in the tissue [42]. In contrast, DESI-MSI can not only differentiates tumors from normal tissue but also provide more detailed information about which lipid molecule contribute to this difference.

The DESI-MSI-based molecular characterisation method described here takes approximately an hour to complete. Moreover, it can directly determine the safe margin distance on fresh frozen sections to a comparable accuracy. The DESI-MSI safe surgical resection distance of most lesions was found to be located in the close margin region (2−10 mm), and only two lesions were located in the negative margin region (> 10 mm). Moreover, DESI-MSI safe surgical resection distances were mainly located in the histopathologically negative margin regions. It has been reported that cancer-related metabolic changes may occur in a region of histological negative margins. Our results validated that the DESI-MSI molecular diagnostic model can individually measure the OSCC safe margin in fresh frozen sections.

To validate the accuracy of the DESI-MSI molecular diagnostic model, we also detected the expression level of p53 in the surgical margin and compared it with the safe surgical resection range determined by DESI-MSI. The results showed that the safe surgical margin boundary determined by the two methods was highly consistent (Table S11). We are pleased to report that our diagnostic model also accurately determined the positive surgical margin distance, which is highly consistent with the histopathological margin distance. These results further confirmed the reliability of the DESI-MSI molecular diagnostic model.

As the DESI-MSI margin analysis was performed in an ambient environment with minimal requirements for specimen preparation, margin-specific molecular information can be well preserved. We believe that this technique has the potential to offer guidance during surgery. Furthermore, it can be performed much more rapidly than histopathological evaluation and can serve as a powerful complement to traditional staining methods. Compared with the traditional mass spectrometry method (such as GC-MS, UHPLC-MS), DESI-MSI provide another possible and powerful tool complementary with the currently available technique in clinical practice. The expense of the DESI-MSI test on one tissue sample is very affordable. The consumption for each test mainly consisted of organic solvent, nitrogen gas, glass slide, and ultrapure water. Based on our previous practice experience, it is estimated that no less than 250 tissue cryosections can be tested given a bottle of 4L solvent, 4L water, a tank of 56 L nitrogen gas. Given the quotation price of acetonitrile ($540, 4L), ultrapure water ($40, 4L), nitrogen gas ($ 268, 56L), and glass slide ($200, 200 sections), the price for each sample can be estimated no more than $5.00. However, it should be noted that the clinical application of the DESI-MSI/Lasso diagnostic model still requires more work. For example, the DESI-MSI molecular diagnostic model needs to be validated in more OSCC specimens. Our study mainly focused on the mucosal margin on the surface and did not thoroughly examine the deep margin. In the future, it is necessary to collect more samples to further study the deep margin and evaluate the ability of characteristic lipid molecules to predict prognosis. Moreover, it also requires the use of an expensive and often bulky mass spectrometer. Nevertheless, more sensitive, efficient, and less expensive mass spectrometers are being developed, and we believe these devices will soon be available for clinical use [43-48].

In conclusion, we successfully constructed a DESI-MSI molecular diagnostic model by combining DESI-MSI and Lasso, which can accurately distinguish different margin statuses and make an individualised measurement of the safe margin distance. The model proposes a new concept of safe margin cut-off in OSCC with every OSCC lesion having its own safe margin cut-off.

Contributors

XHY, QGH, XWS, YHN, and RNZ performed the investigation and project administration for the study. XXZ, XWS, and LZ supplied the resources and software for this study. XWS, SC, YY, and LZ performed the data curation and formal analysis. XXZ and VS contributed to the statistical analysis, and YHN and SW performed validation and visualisation of the data. XHY, XWS, and YHN wrote the original draft, and RNZ and QGH provided subsequent reviews and editing. All authors have read and approved the final manuscript.

Declaration of Competing Interest

Authors declare that they have no competing interests.

Acknowledgements

This study was supported by Jiangsu Provincial Key Medical Discipline (since 2017), Jiangsu Provincial Medical Youth Talent (QNRC2016841), and the National Natural Science Foundation of China (No.81772880, 81702680). The funders had no role in the study design, data collection and analysis, decision to publish, or preparation of the manuscript.

Data sharing statement

The DESI imaging data of all study cases and processing codes are available for open access by request.

Supplementary materials

Supplementary material associated with this article can be found, in the online version, at doi:10.1016/j.ebiom.2021.103529.

References

[1] Ferlay J, Colombet M, Soerjomataram I, Mathers C, Parkin DM, Piñeros M, et al. Estimating the global cancer incidence and mortality in 2018: Globocan sources and methods. Int J Cancer 2019;144(8):1941–53.
[2] Rivera C, Oliveira AK, Costa RAP, De Rossi T, Paes Leme AF. Prognostic biomarkers in oral squamous cell carcinoma: a systematic review. Oral Oncol 2017;72:38–47.
[3] Priya SR, D'Cruz AK, Pai PS. Cut margins and disease control in oral cancers. J Cancer Res Ther 2012;8(1):74–9.
[4] Iseli TA, Lin MJ, Tsui A, Guiney A, Wiesenfeld D, Iseli CE. Are wider surgical margins needed for early oral tongue cancer? J Laryngol Otol 2012;126 (3):289–94.
[5] Binahmed A, Nason RW, Abdoh AA. The clinical significance of the positive surgical margin in oral cancer. Oral Oncol 2007;43(8):780–4.
[6] Sopka DM, Li T, Lango MN, Mehra R, Liu JC, Burtness B, et al. Dysplasia at the margin? Investigating the case for subsequent therapy in 'low-risk' squamous cell carcinoma of the oral tongue. Oral Oncol 2013;49(11):1083–7.
[7] Leemans CR, Tiwari R, Nauta JJ, van der Waal I, Snow GB. Recurrence at the primary site in head and neck cancer and the significance of neck lymph node metastases as a prognostic factor. Cancer 1994;73(1):187–90.
[8] Looser KG, Shah JP, Strong EW. The significance of "positive" margins in surgically resected epidermoid carcinomas. Head Neck Surg 1978;1(2):107–11.
[9] Slaughter DP, Southwick HW, Smejkal W. Field cancerization in oral stratified squamous epithelium; clinical implications of multicentric origin. Cancer 1953;6 (5):963–8.
[10] Mao L, Clark D. Molecular margin of surgical resections—where do we go from here? Cancer 2015;121(12):1914–6.
[11] Chiou WY, Lin HY, Hsu FC, Lee MS, Ho HC, Su YC, et al. Buccal mucosa carcinoma: surgical margin less than 3 mm, not 5 mm, predicts locoregional recurrence. Radiat Oncol 2010;5:79.
[12] Zanoni DK, Migliacci JC, Xu B, Katabi N, Montero PH, Ganly I, et al. A proposal to redefine close surgical margins in squamous cell carcinoma of the oral tongue. JAMA Otolaryngol Head Neck Surg 2017;143(6):555–60.
[13] Dik EA, Willems SM, Ipenburg NA, Adriaansens SO, Rosenberg AJ, van Es RJ. Resection of early oral squamous cell carcinoma with positive or close margins: relevance of adjuvant treatment in relation to local recurrence: margins of 3 mm as safe as 5 mm. Oral Oncol 2014;50(6):611–5.
[14] Nason RW, Binahmed A, Pathak KA, Abdoh AA, Sándor GK. What is the adequate margin of surgical resection in oral cancer? Oral Surg Oral Med Oral Pathol Oral Radiol Endod 2009;107(5):625–9.
[15] Yang XH, Zhang XX, Jing Y, Ding L, Fu Y, Wang S, et al. Amino acids signatures of distance-related surgical margins of oral squamous cell carcinoma. EBioMedicine 2019;48:81–91.
[16] Takáts Z, Wiseman JM, Gologan B, Cooks RG. Mass spectrometry sampling under ambient conditions with desorption electrospray ionization. Science 2004;306 (5695):471–3.
[17] Costa AB, Cooks RG. Simulation of atmospheric transport and droplet-thin film collisions in desorption electrospray ionization. Chem Commun (Camb) 2007 (38):3915–7.
[18] Takáts Z, Wiseman JM, Cooks RG. Ambient mass spectrometry using desorption electrospray ionization (DESI): instrumentation, mechanisms and applications in forensics, chemistry, and biology. J Mass Spectrom 2005;40(10):1261–75.
[19] Wu C, Dill AL, Eberlin LS, Cooks RG, Ifa DR. Mass spectrometry imaging under ambient conditions. Mass Spectrom Rev 2013;32(3):218–43.
[20] Garza KY, Feider CL, Klein DR, Rosenberg JA, Brodbelt JS, Eberlin LS. Desorption electrospray ionization mass spectrometry imaging of proteins directly from biological tissue sections. Anal Chem 2018;90(13):7785–9.
[21] Eberlin LS, Margulis K, Planell-Mendez I, Zare RN, Tibshirani R, Longacre TA, et al. Pancreatic cancer surgical resection margins: molecular assessment by mass spectrometry imaging. PLoS Med 2016;13(8):e1002108.
[22] Eberlin LS, Tibshirani RJ, Zhang J, Longacre TA, Berry GJ, Bingham DB, et al. Molecular assessment of surgical-resection margins of gastric cancer by mass-spectrometric imaging. PNAS 2014;111(7):2436–41.
[23] Johnson RE, Sigman JD, Funk GF, Robinson RA, Hoffman HT. Quantification of surgical margin shrinkage in the oral cavity. Head Neck 1997;19(4):281–6.
[24] Mistry RC, Qureshi SS, Kumaran C. Post-resection mucosal margin shrinkage in oral cancer: quantification and significance. J Surg Oncol 2005;91(2):131–3.
[25] He J, Huang L, Tian R, Li T, Sun C, Song X, et al. MassImager: a software for interactive and in-depth analysis of mass spectrometry imaging data. Anal Chim Acta 2018;1015:50–7.
[26] Huang L, Mao X, Sun C, Luo Z, Song X, Li X, et al. A graphical data processing pipeline for mass spectrometry imaging-based spatially resolved metabolomics on tumor heterogeneity. Anal Chim Acta 2019;1077:183–90.
[27] Friedman JHT, Simon N, Tibshirani R. glmnet: lasso and elastic-net regularized generalized linear models 2013. Available from: https://cran.rproject.org/web/packages/glmnet/index.html.
[28] Tibshirani R. Regression shrinkage and selection via the lasso. J R Stat Soc Ser B (Methodological) 1996;58(1):267–88.
[29] Banerjee S, Zare RN, Tibshirani RJ, Kunder CA, Nolley R, Fan R, et al. Diagnosis of prostate cancer by desorption electrospray ionization mass spectrometric imaging of small metabolites and lipids. PNAS 2017;114(13):3334–9.
[30] Poeta ML, Manola J, Goldwasser MA, Forastiere A, Benoit N, Califano JA, et al. TP53 mutations and survival in squamous-cell carcinoma of the head and neck. N Engl J Med 2007;357(25):2552–61.
[31] Cruz IB, Snijders PJ, Meijer CJ, Braakhuis BJ, Snow GB, Walboomers JM, et al. p53 expression above the basal cell layer in oral mucosa is an early event of malignant transformation and has predictive value for developing oral squamous cell carcinoma. J Pathol 1998;184(4):360–8.
[32] van Houten VM, Leemans CR, Kummer JA, Dijkstra J, Kuik DJ, van den Brekel MW, et al. Molecular diagnosis of surgical margins and local recurrence in head and neck cancer patients: a prospective study. Clin Cancer Res 2004;10(11):3614–20.
[33] Kain JJ, Birkeland AC, Udayakumar N, Morlandt AB, Stevens TM, Carroll WR, et al. Surgical margins in oral cavity squamous cell carcinoma: current practices and future directions. Laryngoscope 2020;130(1):128–38.
[34] Yang XH, Ding L, Fu Y, Chen S, Zhang L, Zhang XX, et al. p53-positive expression in dysplastic surgical margins is a predictor of tumor recurrence in patients with early oral squamous cell carcinoma. Cancer Manag Res 2019;11:1465–72.
[35] Helliwell T, Woolgar J. Standards and minimum datasets for reporting common cancers. Minimum dataset for head and neck histopathology reports. London: The Royal College of Pathologists; 1998.
[36] Calligaris D, Caragacianu D, Liu X, Norton I, Thompson CJ, Richardson AL, et al. Application of desorption electrospray ionization mass spectrometry imaging in breast cancer margin analysis. PNAS 2014;111(42):15184–9.
[37] Pirro V, Alfaro CM, Jarmusch AK, Hattab EM, Cohen-Gadol AA, Cooks RG. Intraoperative assessment of tumor margins during glioma resection by desorption electrospray ionization-mass spectrometry. PNAS 2017;114(26):6700–5.
[38] Eberlin LS, Norton I, Orringer D, Dunn IF, Liu X, Ide JL, et al. Ambient mass spectrometry for the intraoperative molecular diagnosis of human brain tumors. PNAS 2013;110(5):1611–6.
[39] Dill AL, Eberlin LS, Zheng C, Costa AB, Ifa DR, Cheng L, et al. Multivariate statistical differentiation of renal cell carcinomas based on lipidomic analysis by ambient ionization imaging mass spectrometry. Anal Bioanal Chem 2010;398(7-8):2969–78.
[40] Guenther S, Muirhead LJ, Speller AV, Golf O, Strittmatter N, Ramakrishnan R, et al. Spatially resolved metabolic phenotyping of breast cancer by desorption electrospray ionization mass spectrometry. Cancer Res 2015;75(9):1828–37.
[41] Margulis K, Chiou AS, Aasi SZ, Tibshirani RJ, Tang JY, Zare RN. Distinguishing malignant from benign microscopic skin lesions using desorption electrospray ionization mass spectrometry imaging. PNAS 2018;115(25):6347–52.
[42] Kain JJ, Birkeland AC, Udayakumar N, Morlandt AB, Stevens TM, Carroll WR, Rosenthal EL, Warram JM. Surgical margins in oral cavity squamous cell carcinoma: current practices and future directions. Laryngoscope 2020;130(1):128–38.
[43] Ouyang Z, Cooks RG. Miniature mass spectrometers. Annu Rev Anal Chem (Palo Alto Calif) 2009;2:187–214.
[44] Snyder DT, Pulliam CJ, Ouyang Z, Cooks RG. Miniature and fieldable mass spectrometers: recent advances. Anal Chem 2016;88(1):2–29.
[45] Zhang J, Rector J, Lin JQ, Young JH, Sans M, Katta N, et al. Nondestructive tissue analysis for ex vivo and in vivo cancer diagnosis using a handheld mass spectrometry system. Sci Transl Med 2017;9(406).
[46] Schäfer KC, Balog J, Szaniszló T, Szalay D, Mezey G, Dénes J, et al. Real time analysis of brain tissue by direct combination of ultrasonic surgical aspiration and sonic spray mass spectrometry. Anal Chem 2011;83(20):7729–35.
[47] Saudemont P, Quanico J, Robin YM, Baud A, Balog J, Fatou B, et al. Real-time molecular diagnosis of tumors using water-assisted laser desorption/ionization mass spectrometry technology. Cancer Cell 2018;34(5):840–51 e4.
[48] Balog J, Sasi-Szabó L, Kinross J, Lewis MR, Muirhead LJ, Veselkov K, et al. Intraoperative tissue identification using rapid evaporative ionization mass spectrometry. Sci Transl Med 2013;5(194):194ra93.